

Kelp canopy area and biomass from LANDSAT 5

Kyle Cavanaugh, 2011

The Landsat 5 TM sensor has acquired 30 m spatial resolution multispectral imagery nearly continuously from 1984 to the present on a 16-day repeat cycle (Markham et al. 2004). TM obtains data in 7 spectral bands: blue (450-520 nm), green (520-600 nm), red (630-690 nm), near infrared (760-900), shortwave infrared (1500-1750 and 2080-2350 nm), and longwave (thermal) infrared (10400-12500 nm) (<http://landsat.gsfc.nasa.gov/about/tm.html>). TM data is stored as 8-bit encoded radiance, with 256 possible “brightness values” representing the range of radiance for each band. The kelp near infrared (band 4) radiance signal, while strong compared to that of water, spans only the lowest ~40 brightness values detectable by TM. Each Landsat scene covers an area 170 x 180 km; Figure 1 gives an example of the extent of a single scene. During preprocessing, Landsat images were geometrically corrected using ground control points and a digital elevation model to achieve a scene-to-scene registration accuracy < 7.3 m (Lee et al. 2004).

The following describes the automated classification process that we developed in order to consistently and efficiently transform these images into maps of kelp canopy biomass. First, a single orthorectified Landsat TM image was atmospherically corrected to apparent surface reflectance using an atmospheric transmission model (MODTRAN4; Berk et al. 1998). We used this corrected image as a reference and standardized the radiometric signals from all other images to this reference using 50 targets that were assumed to be spectrally stable across the time series (i.e. airport runways, highways,

sand dunes, lakes; Furby & Campbell 2001, Baugh & Groeneveld 2008). Outliers were manually removed to reduce the effects of temporal changes in some of these targets. This ‘target matching’ procedure accounted for all atmospheric, sensor, and processing differences between the scenes and created a time-series of standardized TM imagery.

We estimated kelp canopy abundance from the calibrated Landsat TM reflectance data using multiple endmember spectral mixture analysis (MESMA). Spectral mixture analysis models the fractional cover of two or more “endmembers” within a pixel. Each endmember represents a pure cover type, and endmembers are assumed to combine linearly (Adams et al., 1993). Standard spectral mixture analysis uses a uniform set of endmembers for the entire image. One challenge in the near-shore marine zone is that the “water” reflectance is influenced by sun glint, breaking surface waves, phytoplankton blooms, dissolved organic matter, sediment runoff, etc. Since water reflectance is highly variable in space and time, a single water endmember cannot be used (Figure 2A). Roberts et al. (1998) developed MESMA to allow endmembers to vary on a per-pixel basis. By selecting from multiple endmembers for one or more cover types, MESMA can better capture the spectral variability of the cover type within an image and through time. MESMA has been extensively used for mapping terrestrial vegetation, include aridland vegetation (Okin et al., 2001), shrublands (Dennison and Roberts, 2003a), forests (Youngentob et al., *in review*), and salt marsh (Li et al., 2005).

We modeled pixel reflectance as the linear mixture of reflectance from two endmembers: kelp and water. Thirty water endmembers were selected from non-kelp covered areas within each TM scene using the endmember selection technique described by Dennison and Roberts (2003b). A single kelp endmember was selected by extracting

kelp-covered pixel spectra from each image and finding the single spectrum that fit the entire library of kelp spectra with the lowest root mean square error (RMSE) (Dennison and Roberts, 2003b). The pixels in each TM image were then modeled as a two-endmember mixture of kelp and each of the 30 water endmembers. The final model (out of 30) chosen for each pixel was the model that minimized RMSE when fit to the spectrum of that pixel. The result of this process was a measure of the relative fraction of each pixel that was covered by kelp canopy (Figure 2B). We used a kelp fraction threshold of 0.13 to automate the identification of ‘kelp-covered’ pixels. The multiple endmember process successfully delineated kelp canopy extent under a variety of conditions. Figure 2 provides examples of how our technique retrieved kelp fractions from images that were contaminated by large amounts of sediment runoff (Feb 23, 2005) and high levels of sun glint (July 4, 2006).

The retrieved kelp fractions were then compared to giant kelp canopy biomass observations that were collected by divers at permanent plots maintained by the Santa Barbara Coastal Long Term Ecological Research (SBC LTER) project at the Arroyo Quemado and Mohawk kelp forests (Figure 1). The data and the methods used to measure giant kelp canopy biomass from diver surveys are described in detail in Rassweiler et al. (2008). Briefly, divers measured the length of all fronds along 5 transects (40 x 1 m) within a plot (40 x 40 m) and converted these lengths to biomass using validated length to weight regressions. Each plot was overlapped by four 30 m TM pixels. For each TM image, we compared the mean kelp fraction of these pixels to the diver measured canopy biomass of each plot with a linear regression.

A strong positive linear relationship was found between the Landsat derived kelp fraction index and giant kelp canopy biomass ($r^2 = 0.64$, $p \ll 0.001$, $df = 94$; Figure 3). We restricted our comparisons to canopy biomass rather than total biomass because optical remote sensing only detects floating kelp. Generally canopy biomass is highly correlated to total biomass ($r^2 = 0.92$; unpublished SBC LTER data); however, the relationship between TM kelp fraction and canopy biomass was stronger than between kelp fraction and total biomass ($r^2 = 0.49$, $p \ll 0.001$, $df = 94$). This discrepancy was driven by a few data points where the ratio of canopy to total biomass was unusually low. Neither tidal nor current fluctuations had any effect on the kelp fraction/canopy biomass relationship ($p = 0.65$ and 0.25 when the residuals of the fraction-biomass relationship were compared to local tides and currents for the time of Landsat data collection, respectively). This result agrees with previous work showing that the relatively weak tidal fluctuations and current speeds in this area do not affect remote sensing estimates of kelp biomass as they do in other locations (Cavanaugh et al. 2010 compared to Britton-Simmons et al. 2008). The relationship between satellite derived kelp fraction and diver measured canopy biomass (Figure 3) was used to transform images of kelp fractional cover into quantitative, validated maps of giant kelp canopy biomass. These maps are available every 1 to 2 months for the past 25 years and resolve giant kelp canopy biomass on spatial scales of 30 m to regional scales, which is here defined as the extent of the Landsat 5 TM scene used (Figure 1).

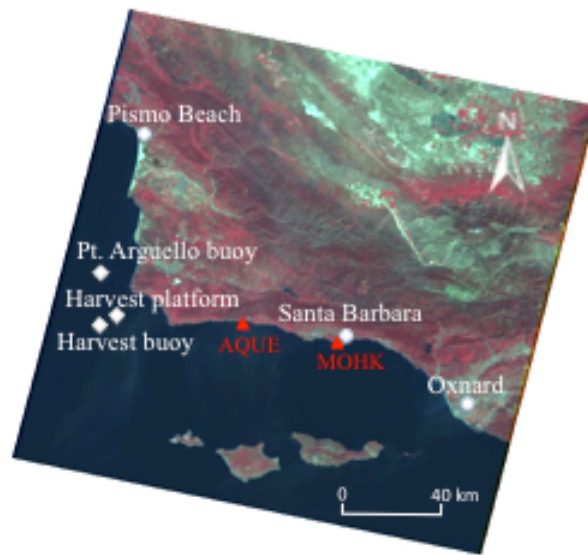


Figure 1. LANDSAT TM scene displaying study area, Pt. Arguello, Harvest, and Harvest Platform buoys, and LTER diver transects at the Arroyo Quemado (AQUE) and Mohawk (MOHK) kelp forests.

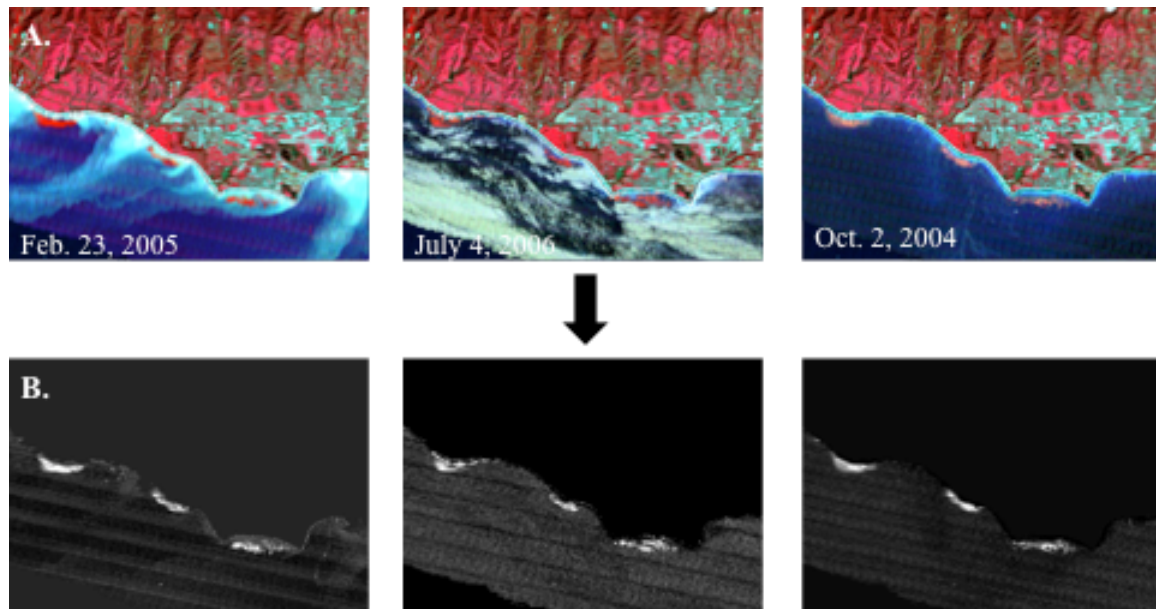


Figure 2. Satellite kelp fraction analysis. (A) LANDSAT false color image of giant kelp beds off Santa Barbara coast. Note variability of water reflectance resulting from sediment runoff in the Feb. 23, 2005 image and glint in the July 4, 2006 image. (B) Kelp fraction images from spectral unmixing process. Brighter pixels correspond to higher kelp fractions. The slight banding apparent in the water is noise that occurs when the detector transitions from bright land targets to dark ocean targets.

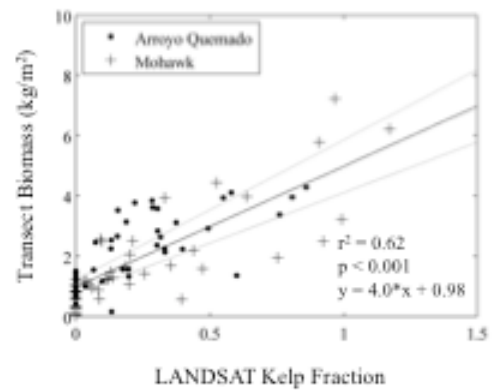


Figure 3. Validation of LANDSAT satellite biomass estimates. Linear regression analysis between LANDSAT kelp fractions and diver measured canopy biomass (kg/m^2) measurements for Arroyo Quemado and Mohawk ($n=96$). The gray lines represent 95% confidence intervals for the relationship.

References

- Adams J, Smith M, Gillespie A (1993) Imaging spectroscopy: Interpretation based on spectral mixture analysis. *Remote geochemical analysis: Elemental and mineralogical composition* 7:145-166
- Baugh W, Groeneveld D (2008) Empirical proof of the empirical line. *International Journal of Remote Sensing* 29:665-672
- Berk A, Bernstein L, Anderson G, Acharya P, Robertson D, Chetwynd J, Adler-Golden S (1998) MODTRAN cloud and multiple scattering upgrades with application to AVIRIS - editions of 1991 and 1992. *Remote Sensing of Environment* 65:367-375
- Britton-Simmons K, Eckman J, Duggins D (2008) Effect of tidal currents and tidal stage on estimates of bed size in the kelp *Nereocystis luetkeana*. *Marine Ecology-Progress Series* 355:95
- Cavanaugh K, Siegel D, Kinlan B, Reed D (2010) Scaling giant kelp field measurements to regional scales using satellite observations. *Marine Ecology Progress Series* 403:13-27
- Dennison P, Roberts D (2003a) The effects of vegetation phenology on endmember selection and species mapping in southern California chaparral. *Remote Sensing of Environment* 87:295-309
- Dennison P, Roberts D (2003b) Endmember selection for multiple endmember spectral mixture analysis using endmember average RMSE. *Remote Sensing of Environment* 87:123-135
- Furby S, Campbell N (2001) Calibrating images from different dates to 'like-value' digital counts. *Remote Sensing of Environment* 77:186-196
- Lee D, Storey J, Choate M, Hayes R (2004) Four years of Landsat-7 on-orbit geometric calibration and performance. *IEEE Transactions on Geoscience and Remote Sensing* 42:2786-2795
- Li L, Ustin S, Lay M (2005) Application of multiple endmember spectral mixture analysis (MESMA) to AVIRIS imagery for coastal salt marsh mapping: A case study in China Camp, CA, USA. *International Journal of Remote Sensing* 26:5193-5207

- Markham B, Storey J, Williams D, Irons J (2004) Landsat sensor performance: history and current status. *Geoscience and Remote Sensing, IEEE Transactions* 42:2691-2694
- Okin G, Roberts D, Murray B, Okin W (2001) Practical limits on hyperspectral vegetation discrimination in arid and semiarid environments. *Remote Sensing of Environment* 77: 212-225
- Rassweiler A, Arkema K, Reed D, Zimmerman R, Brzezinski M (2008) Net primary production, growth, and standing crop of *Macrocystis pyrifera* in southern California. *Ecology* 89:2068-2068
- Roberts D, Gardner M, Church R, Ustin S, Scheer G, Green R (1998) Mapping chaparral in the Santa Monica Mountains using multiple endmember spectral mixture models. *Remote Sensing of Environment* 65:267-279
- Youngentob K, Roberts D, Held A, Dennison P, Jia X, Lindenmayer D, Mapping two *Eucalyptus* subgenera using multiple endmember spectral mixture analysis and continuum-removed imaging spectrometry data. *Remote Sensing of Environment*, in review, accepted with minor revisions.